
HRP: High-Rank Preheating for Superior LoRA Initialization

Yuzhu Chen¹ Yingjie Wang² Shi Fu^{1,2} Li Shen³ Yongcheng Jing² Xinmei Tian¹ Dacheng Tao²

Abstract

This paper studies the crucial impact of initialization on the convergence properties of Low-Rank Adaptation (LoRA). We theoretically demonstrate that random initialization, a widely used schema, will likely lead LoRA to random low-rank results, rather than the best low-rank result. While this issue can be mitigated by adjusting initialization towards a well-informed direction, it relies on prior knowledge of the target, which is typically unknown in real-world scenarios. To approximate this well-informed initial direction, we propose High-Rank Preheating (HRP), which fine-tunes high-rank LoRA for a few steps and uses the singular value decomposition of the preheated result as a superior initialization. HRP initialization is theory-supported to combine the convergence strengths of high-rank LoRA and the generalization strengths of low-rank LoRA. Extensive experiments demonstrate that HRP significantly enhances LoRA’s effectiveness across various models and tasks, achieving performance comparable to full-parameter fine-tuning and outperforming other initialization strategies.

1. Introduction

Recent advances in foundational models, especially large language models, have achieved remarkable success in a diverse range of applications (Bommasani et al., 2021; Touvron et al., 2023; Achiam et al., 2023; Fu et al., 2024a;b). Nevertheless, owing to their substantial scale, the conventional full-parameter fine-tuning (FPFT) approach, in which all the model’s parameters are updated for specialized tasks, has become progressively more formidable and inefficient. Parameter-efficient fine-tuning methods concentrate on selectively updating smaller parameter subsets or integrating

lightweight adapters, thus substantially diminishing computational and storage demands (Hu et al., 2021; Liu et al., 2022; Kumar et al., 2022). This transition not only renders the fine-tuning process more tractable but also unlocks new prospects for deploying these potent models in resource-constrained settings.

A leading technique in this area is Low-Rank Adaptation (LoRA) (Hu et al., 2021), which introduces lightweight low-rank adapters to the pre-trained weight matrices. LoRA has been extensively applied and has manifested substantial achievements in tailoring large language models (Hu et al., 2021; Mao et al., 2025) and image generation models (Filatov & Kindulov, 2023; Ji et al., 2024) for a variety of downstream applications. Although LoRA presents significant computational benefits in practical scenarios, it still proves less effective than FPFT when efficiency is not a primary consideration (Biderman et al., 2024).

To enhance LoRA’s effectiveness, many variants have emerged, with initialization improvement being one line of approach. In classic LoRA, one adapter is initialized with a zero matrix and the other with a random matrix. This causes the fine-tuning process to commence from the pre-trained weights. However, due to the random-initialized adapter, the fine-tuning process begins with a random direction. Methods like PiSSA (Meng et al., 2024) and LoRA-GA (Wang et al., 2024) use Singular Value Decomposition (SVD) of pre-trained weights and gradients for initialization, proving its significance in LoRA’s performance. However, these methods rely heavily on pre-trained models and lack theoretical guarantees for better performance, calling for more research to optimize LoRA.

Delving into the optimization landscape of LoRA, this paper theoretically demonstrates that initialization plays a crucial role in achieving optimal performance. Nevertheless, random initialization methods cause the adapters to be initialized from a random direction, which leads to sub-optimal fine-tuning results with high probability. To address this issue, we propose High-Rank Preheating (HRP), an initialization enhancement algorithm. It uses a few steps of high-rank LoRA as a preheating step for wise initialization before the real low-rank LoRA optimization. HRP not only inherits the convergence advantages related to high-rank LoRA but also keeps good generalization properties from low-rank LoRA

¹University of Science and Technology, Hefei, China
²Nanyang Technological University, Singapore ³Sun Yat-sen University, Guangzhou, China. Correspondence to: Yuzhu Chen <cyzkrau@mail.ustc.edu.cn>, Dacheng Tao <dacheng.tao@gmail.com>.

by keeping the number of trainable parameters small.

Our contributions can be summarized as follows:

1. On the theory side, we demonstrate that initialization is important for LoRA to converge to optimal results. We analyze the gradient flow of classic LoRA and Asymmetric LoRA, one LoRA variant that only updates the zero-initialized matrices. We demonstrate that 1) with random initialization, Asymmetric LoRA hardly converges to the best low-rank approximation when approximating a matrix, 2) classic LoRA has a similar dynamic with Asymmetric LoRA in fine-tuning schema and also can not converge well from some initialization, and 3) with wise initialization, both Asymmetric LoRA and classic LoRA converges exponentially to the best low-rank approximation.
2. On the algorithm side, we propose High-Rank Preheating (HRP), a LoRA initialization algorithm to approach the wise initialization suggested in theory. In addition to the main LoRA with low rank, HRP further employs a few steps of Asymmetric LoRA optimization as preheating and treats the SVD decomposition of preheated adapters as approximations of targets' SVD decomposition, which is guaranteed to converge well. With only modification in initialization, HRP is theory-guaranteed to make LoRA achieve convergence power comparable to high-rank LoRA (preheating stage) while preserving generalization properties due to maintaining the same number of trainable parameters.
3. On the experimental side, we conducted experiments on neural language understanding (NLU) tasks and neural language generation (NLG) tasks across various models to evaluate the effectiveness of HRP. In NLU tasks, classic LoRA with HRP outperforms its other variants and achieves comparable performance with full-parameter fine-tuning, Asymmetric LoRA with HRP outperforms other initialization methods and achieves comparable performance with classic LoRA while holding about half trainable parameters in main optimization.

2. Related Work

In this section, we provide an overview of the related work, including works on the analysis of initialization, LoRA variations, and theory results about matrix sensing.

2.1. Role of initialization

Parameter initialization is one of the initial elements that largely account for the final model performance (Glorot &

Bengio, 2010; Mishkin & Matas, 2015). Existing initialization methods are designed to control the norms of network parameters via Gaussian initialization (He et al., 2015) or orthonormal matrix initialization (Saxe et al., 2013) with different variance patterns. Currently, learning-based initialization methods are explored: Dauphin & Schoenholz (2019) propose to optimize the curvature, Zhu et al. (2021) suggest optimizing the loss reduction of the first stochastic step, while Yang et al. (2022) optimize the cosine similarity of sample-wise gradients.

The initialization for LoRA is also a hot topic in previous research. Hayou et al. (2024a) study the difference between the left sketch and the right sketch from a stability perspective. Büyükakyüz (2024) leverage orthonormal matrix initialization through QR decomposition. Meng et al. (2024); Wang et al. (2024) initialize adapters with the principal components of the weight matrices and their gradients in pre-trained models. Li et al. (2024) bring Nyström initialization to LoRA for better convergence. Compared to these works, our method does not require further knowledge about the pre-trained weights or the gradient.

2.2. LoRA variations

Since the introduction of the original LoRA technique (Hu et al., 2021), there are various efforts to enhance LoRA further. Zhang et al. (2023) adaptively allocate the parameter budget among weight matrices. Zhu et al. (2024) freeze the random-initialized matrices for better generalization. Xia et al. (2024); Malinovsky et al. (2024) suggest using a chain of LoRA for better expressive power. To further decrease the number of trainable parameters, Bałazy et al. (2024); Ponkshe et al. (2024) suggest injecting small matrices between LoRA blocks and Kopiczko et al. (2023); Renduchintala et al. (2023); Song et al. (2024) suggest sharing LoRA weights across different modules. Compared to these works, this paper focuses on enhancing LoRA from the perspective of initialization.

2.3. Matrix sensing

We also note some works about matrix sensing here. Matrix sensing considers approximating a low-rank matrix by two multiplied matrices (Chi et al., 2019). Theoretical works show that this training paradigm converges in both symmetric (Tarmoun et al., 2021; Min et al., 2021) and asymmetric (Ye & Du, 2021; Wind, 2023) settings when adapters are initialized to small random matrices. Compared to these works, this paper focuses more on the realistic setting for LoRA, where the target may have a high rank and initialization is not small.

3. Theory: Why Initialization Matters

In this section, we investigate LoRA’s gradient flow, demonstrating how its initialization influences convergence.

3.1. Framework

LoRA (Hu et al., 2021) adapts pre-trained models by updating weights through the product of two low-rank matrices scaled by a multiplier. Specifically, for a sub-module $W^{\text{pre}} \in \mathbb{R}^{b \times a}$ in the pre-trained model, r -rank LoRA uses $A \in \mathbb{R}^{a \times r}$ and $B \in \mathbb{R}^{b \times r}$ as adapters, and the weight adaption is given by

$$W^{\text{pre}} \rightarrow W^{\text{pre}} + \frac{\alpha}{r} B A^\top,$$

where α denotes the scaling factor. During the fine-tuning process, the original weights W^{pre} are kept frozen, while the parameters of A and B are updated through optimization algorithms.

In this paper, we study the gradient flow of A and B , which approximates gradient descent. For loss function \mathcal{L} , the update rule of gradient descent is given by:

$$\begin{aligned} A_{t+1} &= A_t - \frac{\eta_A \alpha}{r} \nabla_W \mathcal{L}(W + \frac{\alpha}{r} B_t^\top A_t)^\top B_t, \\ B_{t+1} &= B_t - \frac{\eta_B \alpha}{r} \nabla_W \mathcal{L}(W + \frac{\alpha}{r} B_t^\top A_t) A_t, \end{aligned}$$

where η_A is the learning rate for optimizing A while η_B is for B . When the learning rate is sufficiently small, the update rule is a first-order approximation of the following gradient flow:

$$\begin{cases} \dot{A}_t = -\frac{\eta_A \alpha}{r} \nabla_W \mathcal{L}(W + \frac{\alpha}{r} B_t^\top A_t)^\top B_t, \\ \dot{B}_t = -\frac{\eta_B \alpha}{r} \nabla_W \mathcal{L}(W + \frac{\alpha}{r} B_t^\top A_t) A_t, \end{cases} \quad (1)$$

where the notion \dot{A}_t denotes $\frac{dA_t}{dt}$ and \dot{B}_t is defined similarly.

LoRA is widely used with a **zero+random initialization schema**, where one adapter is initialized to a zero matrix and another to a random matrix. Every element in the random initialized matrix is independently and identically distributed from a Gaussian distribution $\mathcal{N}(0, \sigma^2)$. We call the $A_0 = O_{a \times r}$ case left sketch initialization (LSI) and the $B_0 = O_{b \times r}$ case right sketch initialization (RSI). Zhu et al. (2024) suggest orthogonal initialization, which replaces the Gaussian matrix with its r singular vectors and demonstrates similar performance to Gaussian initialization.

Updating A and B with different learning rates is suggested by Hayou et al. (2024b), however, A and B are updated with the same learning rate in classic LoRA. Another variant is Asymmetric LoRA, as proposed by Zhu et al. (2024), suggests freezing the random-initialized matrix while only updating the zero-initialized matrix for better generalization. In this paper, we consider two settings: 1) **classic LoRA**

where $\eta_A = \eta_B = \eta$, and 2) **Asymmetric LoRA** where $\eta_A = 0, \eta_B = \eta$ for RSI and $\eta_A = \eta, \eta_B = 0$ for LSI.

We note that for LoRA, what matters fine-tuning performance is the after-multiplied adapter $X_t = \frac{\alpha}{r} B_t A_t^\top$, rather than exact values of A_t or B_t . For analyzing the dynamic of X_t , we further consider auxiliary matrices $Y_t = \frac{\alpha}{r} A_t A_t^\top$, $Z_t = \frac{\alpha}{r} B_t B_t^\top$, and $G_t = \nabla_W \mathcal{L}(W + X_t)$. Then, optimizing A and B via differential equations 1 is equivalent to optimizing X, Y, Z via the following differential equations:

$$\begin{cases} \dot{X}_t = -\eta_A Z_t G_t - \eta_B G_t Y_t, & X_0 = \frac{\alpha}{r} B_0 A_0^\top, \\ \dot{Y}_t = -\eta_A X_t^\top G_t - \eta_A G_t^\top X_t, & Y_0 = \frac{\alpha}{r} A_0 A_0^\top, \\ \dot{Z}_t = -\eta_B X_t G_t^\top - \eta_B G_t X_t^\top, & Z_0 = \frac{\alpha}{r} B_0 B_0^\top. \end{cases} \quad (2)$$

3.2. Random initialization leads bad convergence

As studied in (Zeng & Lee, 2023), the expressive power of LoRA for fully connected neural networks and the Transformer architecture requires the capability of achieving the best low-rank approximation to some well-trained sub-modules during optimization (the analysis is optimization-free and thus also applicable for Asymmetric LoRA). Formally, for a target model W^{target} , adapter $X_t = \frac{\alpha}{r} B_t A_t^\top$ is expected to achieve the best rank- r approximation of $W^{\text{target}} - W^{\text{pre}}$.

Here we analyze the setting of matrix sensing, where the loss function is the Frobenius norm toward the target. With no loss to generality, we consider $W^{\text{pre}} = O_{b \times a}$ while treating $M = W^{\text{target}} - W^{\text{pre}}$ as target for X_t . Then, the loss function \mathcal{L} and gradient G_t (w.r.t. $X_t = \frac{\alpha}{r} B_t A_t^\top$) can be expressed as

$$\mathcal{L} = \frac{1}{2} \left\| \frac{\alpha}{r} B A^\top - M \right\|_F^2, \quad \text{and} \quad G_t = X_t - M. \quad (3)$$

According to Eckart-Young Theorem (Eckart & Young, 1936), the global minima to this problem is the best rank- r approximation of M , with minimum loss as follows:

$$\mathcal{L}^* = \frac{1}{2} \sum_{i=r+1}^{\min\{a,b\}} \sigma_i(M)^2$$

where $\sigma_i(M)$ is the i -th large singular value of M and we assume non-zero singular values of M are different from each other. For expressive power in more complex tasks, LoRA is expected to at least converge to some points with loss similar to \mathcal{L}^* in the setting of matrix sensing. Unfortunately, we show that fine-tuned results of Asymmetric LoRA and classic LoRA are likely to have a significantly higher loss.

Asymmetric LoRA struggles to converge well. We begin by examining the optimization landscape of Asymmetric LoRA (Zhu et al., 2024), which distinguishes itself from

the classic LoRA by keeping the random-initialized matrix from being updated. Compared to the classic LoRA with an equivalent rank, Asymmetric LoRA results in a reduction of trainable parameters, thereby enhancing generalization capabilities. Its success in experiments demonstrates that the frozen parameters do not substantially compromise the convergence of classic LoRA.

Through analysis of Asymmetric LoRA, we show that under zero+random initialization schema, it is likely to have converged results with loss much higher than \mathcal{L}^* . Specifically, we have the following theorems.

Theorem 3.1. *Consider Asymmetric LoRA under objective 3 with Gaussian initialization and orthogonal initialization. With LSI and RSI in zero+random schema, we have:*

$$\mathbb{E}_{LSI} \left[\mathcal{L}(\lim_{t \rightarrow \infty} X_t) \right] = \frac{b-r}{2b} \sum_{i=1}^{\min\{a,b\}} \sigma_i(M)^2,$$

$$\mathbb{E}_{RSI} \left[\mathcal{L}(\lim_{t \rightarrow \infty} X_t) \right] = \frac{a-r}{2a} \sum_{i=1}^{\min\{a,b\}} \sigma_i(M)^2,$$

where \mathbb{E} represents the expectation with respect to randomness in initialization.

Proof is included in Appendix A.1. Theorem 3.1 shows that under zero+random initialization schema, the expected loss of converged result is the loss of a random rank- r approximation to M , rather than that of best rank- r approximation. This is severe when the target is also of low rank because singular values diverge a lot for low-rank matrices. As observed by Wang et al. (2023), the rank-dimension ratio of well-trained neural networks is usually relatively small, indicating a low-rank structure for W^{pre} and W^{target} , thus also for $M = W^{\text{target}} - W^{\text{pre}}$. Therefore, under random initialization schema, the loss of converged results of Asymmetric LoRA is high in expectation.

Theorem 3.1 also demonstrates that when Asymmetric LoRA is configured with higher ranks, the loss for converged results decreases and performance is enhanced. Specifically, when using Asymmetric LoRA with full rank ($r = \min a, b$), it can converge to zero-loss minima in expectation. However, in practical applications, LoRA typically uses much smaller ranks to reduce memory usage and improve generalization, which results in poor convergence.

Theorem 3.2. *Under the conditions of Theorem 3.1, with the additional assumption that $r < \min a, b$, we have:*

$$\Pr \left[\mathcal{L}(\lim_{t \rightarrow \infty} X_t) = \mathcal{L}^* \right] = 0,$$

where \Pr represents the probability with respect to randomness in initialization.

Proof is included in Appendix A.2. Aside from the high expected loss, Theorem 3.2 further reveals that Asymmetric

LoRA has zero probability of converging to the optimal rank- r approximation of M in matrix sensing problems. This indicates that the high expected loss is not merely due to occasional poor outcomes, but rather stems from the inherent nature of zero+random initialization Asymmetric LoRA to converge to arbitrary low-rank solutions.

Compared with other theoretical works in matrix sensing (Tarmoun et al., 2021; Min et al., 2021; Ye & Du, 2021; Wind, 2023), which demonstrates that the gradient flow of matrix sensing converges to global minima, our approach suggests a different conclusion because of difference in the following ways: 1) we allow the target matrix M to be of high rank, which may not be fully approximate-able by a low-rank matrix X ; 2) we consider the case where adapter matrices are initialized as zero and random, respectively, whereas the aforementioned works assume both matrices are initialized with small random values; and 3) our objective is Asymmetric LoRA, where only one matrix is optimized, which is different from their approaches.

Classic LoRA has similar properties. Different from Asymmetric LoRA, classic LoRA lets the random-initialized to be updated, thus has more trainable parameters and is thus more expressive. Though theory papers in matrix sensing (Tarmoun et al., 2021; Min et al., 2021; Ye & Du, 2021; Wind, 2023) suggest that optimizing both A and B results in convergence to M with high probability under initialization where both A and B are initialized from small random matrices, we demonstrate that under zero+random initialization and fine-tuning schema, classic LoRA also struggles to converge well. First, we show that for some special initialization, classic LoRA also fails to converge to the best low-rank result in matrix sensing.

Theorem 3.3. *For objective 3, if there exists $i \leq r$ making A, B with $A^\top v_i = O_a, B^\top u_i = O_b$. Then classic LoRA under LSI with $A_0 = A, B_0 = O_{b \times r}$ or RSI with $A_0 = O_{a \times r}, B_0 = B$, we have for any t :*

$$X_t v_i = O_b, \quad \text{and} \quad X_t^\top u_i = O_a,$$

resulting in

$$\mathcal{L}(X_t) - \mathcal{L}^* \geq \frac{1}{2} [\sigma_i(M)^2 - \sigma_{r+1}(M)^2] > 0,$$

where $M = U_M \Sigma_M V_M^\top$ is the SVD decomposition of M and u_i, v_i are the i -th column of U, V .

Proof is included in Appendix A.3. Theorem 3.3 shows that when the initialization of LoRA lies on a subspace orthogonal to some $u_i v_i^\top$ in the target, the orthogonal property will always hold in X_t , leading to a failure in converging to the best low-rank result. Target is always unknown in the initializing stage, thus these bad directions can not be easily avoided from random initialization.

Aside from these specific initialization directions that cause poor convergence, we also show that in many fine-tuning cases, classic LoRA has a similar optimization dynamic with Asymmetric LoRA, thus sharing similar properties about bad convergence. This similar dynamic is empirically supported by experiments (Zhu et al., 2024) where Asymmetric LoRA obtains similar results with classic LoRA in real-world scenarios.

Theorem 3.4. *For the gradient flow of classic LoRA $\{X_s\}_{0 \leq s \leq t}$ and the gradient flow of Asymmetric LoRA \tilde{X}_t , assume $\{X_s\}_{0 \leq s \leq t}$ is bounded by R and the computed gradient $X_t \rightarrow G_t$ is Lipschitz in the Frobenius norm (same gradient calculator for classic LoRA and Asymmetric LoRA), then the difference between \tilde{X}_t and X_t is upper bounded by*

$$\|X_t - \tilde{X}_t\|_F = O(\eta R^3 t^2), \quad (4)$$

when they have the same initialization in LSI or RSI.

Proof is included in Appendix A.4. In fine-tuning tasks, pre-trained models have already acquired powerful capabilities from training on other tasks, enabling their effectiveness in real-world applications. Therefore, the fine-tuning stage is expected to make only modest modifications to the model parameters, making the assumption of bounded X_t reasonable. Additionally, assuming the gradient calculator is Lipschitz in the Frobenius norm is justified because the backward propagation process of neural networks exhibits this property in bounded domains. Besides, this Lipschitz assumption is widely adopted in other theoretical works (Patel et al., 2022).

Theorem 3.4 tells that in fine-tuning tasks, classic LoRA has a similar dynamic of Asymmetric LoRA, especially when training is insufficient (with small t). As addressed above, Asymmetric LoRA is likely to get random low-rank results rather than the best low-rank result. With a similar dynamic, classic LoRA also suffers from it.

Theorem 3.4 tells that in fine-tuning tasks, classic LoRA exhibits dynamics similar to those of Asymmetric LoRA, particularly during the early stages of training (small t). As addressed above, Asymmetric LoRA tends to converge to arbitrary low-rank solutions rather than the optimal low-rank approximation under zero+random initialization schema. Given this dynamic similarity, classic LoRA inherits the same limitation.

3.3. Wise initialization leads good convergence

Then, we illustrate that the observed limitation in convergence is mainly attributed to initialization, rather than the training methods. In fact, we show that by merely altering the random initialization to a more informed one, both Asymmetric LoRA and classic LoRA exhibit exponential convergence in the matrix sensing problem. Specifically, we present the following theorems.

Theorem 3.5. *For Asymmetric LoRA under objective 3 in RSI with $A_0 = V_M[:, :r]$, $B_0 = O_{b \times r}$ or LSI with $A_0 = O_{a \times r}$, $B_0 = U_M[:, :r]$, we have*

$$\mathcal{L}(X_t) - \mathcal{L}^* = O(\exp\{-\eta t\}),$$

where $M = U_M \Sigma_M V_M^\top$ is the SVD decomposition of M .

Proof is included in Appendix A.5. Theorem 3.5 shows that when initialized with the principal singular vectors of the target, optimizing with Asymmetric LoRA has exponential convergence to the best low-rank approximation of M . This result contrasts with Theorem 3.1 and Theorem 3.2 solely in terms of the initialization method. Therefore, the problem of convergence limitation of Asymmetric LoRA is attributed to random initialization. Furthermore, when the initialization is appropriately configured, optimizing a single LoRA adapter while frozen another one is sufficient to ensure convergence in matrix sensing.

Theorem 3.6. *For classic LoRA under objective 3 in RSI with $A_0 = V_M[:, :r]$, $B_0 = O_{b \times r}$ or LSI with $A_0 = O_{a \times r}$, $B_0 = U_M[:, :r]$, we have*

$$\mathcal{L}(X_t) - \mathcal{L}^* = O(\exp\{-(1 + k\sigma_r(M))\eta t\}),$$

where $M = U_M \Sigma_M V_M^\top$ is the SVD decomposition of M and $k = \frac{\sqrt{1+4\sigma_1(M)}-1}{\sigma_1(M)} > 0$.

Proof is included in Appendix A.6. Theorem 3.6 demonstrates that with the same initialization, the classic LoRA method is also guaranteed to converge to the best low-rank approximation of M , thereby avoiding the unfavorable scenario described in Theorem 3.3. It is also noteworthy that in this initialization, classic LoRA has a higher convergence rate than Asymmetric LoRA in the context of matrix sensing, while both converging to the best low-rank result.

In practice with pre-trained model modules W^{pre} and its well fine-tuned version W^{target} , LoRA is expected to make each $\frac{\alpha}{r} B_i A_i^\top$ a best low-rank approximation of $W_i^{\text{target}} - W_i^{\text{pre}}$. However, calculating the SVD decomposition of $W_i^{\text{target}} - W_i^{\text{pre}}$ is always impossible because (W_i^{target}) is unknown.

Previous work proposes some initialization methods for LoRA, such as PiSSA and LoRA-GA (Meng et al., 2024; Wang et al., 2024). PiSSA (Meng et al., 2024) considers using SVD decomposition of W^{pre} as initialization while LoRA-GA (Wang et al., 2024) suggests using SVD decomposition of $\nabla_{W^{\text{pre}}} \mathcal{L}(W^{\text{pre}})$. Their methods rely heavily on W_i^{pre} and is not theoretically guaranteed for better convergence.

4. Method: High-Rank Preheating

In this section, we introduce High-Rank Preheating (HRP, Algorithm 4), our proposed LoRA initialization algorithm

for addressing the weaknesses identified in Section 3.

The target of HRP is approaching the wise initialization suggested in Section 3.3, which makes both Asymmetric LoRA and classic LoRA theoretically guaranteed to converge better in matrix sensing. This initialization is not directly available because W^{pre} is unknown. However, through HRP, it can be approximated by using a few steps of high-rank LoRA. Specifically, HRP can be decomposed into two stages: the preheating stage and the initializing stage.

In the preheating stage, HRP uses high-rank LoRA to approximate the main singular vectors of $W^{\text{target}} - W^{\text{pre}}$ as preheating. Using high-rank LoRA is inspired by Theorem 3.1, which tells that LoRA with higher rank has better-converged results in expectation. What we want from high-rank LoRA is an approximation of the main singular vectors of $W^{\text{target}} - W^{\text{pre}}$, which is achieved by main singular values of $\hat{B}\hat{A}^\top$. However, these singular values emerge at the beginning stage of high-rank LoRA optimization, which means a few steps of optimization of high-rank LoRA are enough for preheating.

In the initializing stage, HRP calculates the SVD decomposition of $\hat{B}\hat{A}^\top = U\Sigma V^\top$ and treats $U[:, :r], V[:, :r]$ as an approximation of left and right main singular vectors of $W_i^{\text{target}} - W_i^{\text{pre}}$. Then, HRP injects LoRA into target modules with initialization

$$\begin{aligned} \text{LSI} : A_0 &= O_{a \times r}, \quad B_0 = U[:, :r], \\ \text{RSI} : A_0 &= V[:, :r], \quad B_0 = O_{b \times r}. \end{aligned}$$

If HRP approximates the main singular vectors of $W^{\text{target}} - W^{\text{pre}}$ well, HRP is expected to achieve better results in practice. However, it is also constrained by the limitation of high-rank LoRA. To address this problem, we re-analyze the matrix sensing problem and find that at least, HRP makes low-rank LoRA have comparable convergence properties with high-rank LoRA. Specifically, we have the following theorem.

Theorem 4.1. *For HRP initialized Asymmetric LoRA with one pre-heating step and the same updating rules (LSI preheating with LSI fine-tuning or RSI preheating with RSI fine-tuning) under problem 3, if $\text{rank}(M) \leq r$ we have*

$$\begin{aligned} \mathbb{E}_{\text{LSI}} \left[\mathcal{L}(\lim_{t \rightarrow \infty} X_t) \right] &= \frac{b-R}{2b} \sum_{i=1}^r \sigma_i(M)^2, \\ \mathbb{E}_{\text{RSI}} \left[\mathcal{L}(\lim_{t \rightarrow \infty} X_t) \right] &= \frac{a-R}{2a} \sum_{i=1}^r \sigma_i(M)^2, \end{aligned}$$

where R is the rank at the preheating stage while r is the rank at the real optimizing stage.

Proof is included in Appendix A.7. Theorem 4.1 tells that when target M is also of low rank, HRP makes the expected

Algorithm 1 HRP: High-Rank Preheating

input Rank R and #steps S for preheating, rank r and #steps s for fine-tuning, pre-trained model W

1: High-rank preheating

$$\hat{A}, \hat{B} \leftarrow \text{AsymLoRA}(\hat{A}_0, \hat{B}_0, S)$$

2: Calculate SVD decomposition $U\Sigma V^\top = \hat{B}\hat{A}^\top$

3: Re-initialize

$$\text{RSI: } A_0 = V[:, :r], B_0 = O_{b \times r}$$

or

$$\text{LSI: } A_0 = O_{a \times r}, B_0 = U[:, :r]$$

4: Fine-tuning $A, B \leftarrow \text{LoRA}(A_0, B_0, S)$

output fine-tuned model $W + BA^\top$

loss of converged result decrease to the same as Asymmetric LoRA with rank R , which could improve a lot from zero+random initialization when high rank R is well-settled. Specifically, when preheating LoRA is a full-rank adapter, HRP achieves the wise initialization suggested in Theorem 3.5. We also note that assuming $W^{\text{target}} - W^{\text{pre}}$ to have a low rank is reasonable in practice. Wang et al. (2021; 2023) observe a stabilizing effect in the stable ranks of neural network layers during training, indicating both W^{pre} and W^{target} having small stable rank.

Beyond its convergence advantages, HRP maintains the same number of trainable parameters as low-rank LoRA, thereby preserving the strong generalization properties that mitigate the risk of overfitting. Furthermore, no more trainable parameters also ensure that after a few steps of preheating, HRP requires no additional memory during optimization, retaining the computational benefits that make low-rank LoRA particularly attractive for fine-tuning tasks.

5. Experiments

In this section, we validate the effectiveness of HRP through experiments. We evaluate the performance of HRP and other LoRA variants under the neural language understanding (NLU) tasks (GLUE (Wang, 2018)) on T5-base model (Rafael et al., 2020) and the neural language generation (NLG) tasks (MetaMathQA (Yu et al., 2023), GSM8k (Cobbe et al., 2021), and MATH (Hendrycks et al., 2021a)) on Llama2-7B model (Touvron et al., 2023), Qwen2-7B model (Yang et al., 2024), and Falcon3-7B model (Team, 2024).

We compare HRP with several baselines to demonstrate its effectiveness:

1. Full-Parameter Fine-Tuning (FPFT): the straightforward fine-tuning method, which updates model param-

Table 1. Results with T5-base on tasks from a subset of GLUE benchmark. We report the Matthews correlation coefficient for CoLA, Pearson correlation coefficient for STS-B, and accuracy for the remaining tasks. Results are averaged over 3 seeds and standard deviations are given in the subscript. **Blue bold** marked denotes the best result across different LoRA initialization, and **red bold** marked denotes the best result overall baseline.

	CoLA	MRPC	QNLI	RTE	SST-2	STS-B	Avg.
AdaLoRA	22.44 \pm 17.33	68.06 \pm 0.46	88.23 \pm 0.18	51.02 \pm 2.64	91.70 \pm 0.19	25.53 \pm 7.21	57.83 \pm 2.49
rsLoRA	43.84 \pm 1.22	70.10 \pm 0.20	86.53 \pm 0.32	55.11 \pm 2.13	91.09 \pm 0.48	20.59 \pm 8.65	61.21 \pm 1.19
DoRA	38.79 \pm 3.16	69.53 \pm 0.31	87.19 \pm 0.10	55.23 \pm 2.84	91.74 \pm 0.37	13.38 \pm 3.03	59.31 \pm 0.72
FPFT	51.17 \pm 2.00	86.27\pm0.60	89.65 \pm 0.22	64.62\pm2.70	92.13 \pm 0.38	89.22\pm0.28	78.84\pm0.91
LoRA(Gauss)	54.00 \pm 0.53	73.45 \pm 3.01	90.89 \pm 0.10	57.76 \pm 0.78	92.89 \pm 0.50	85.68 \pm 0.38	75.78 \pm 0.49
LoRA(Orth)	53.39 \pm 1.10	73.77 \pm 0.53	90.83 \pm 0.21	57.64 \pm 1.12	92.89 \pm 0.16	85.87 \pm 0.48	75.73 \pm 0.47
PiSSA	53.12 \pm 0.21	76.63 \pm 5.60	91.34 \pm 0.13	56.80 \pm 0.34	93.35\pm0.32	86.53 \pm 0.37	76.29 \pm 0.90
LoRA-GA	52.62 \pm 1.34	78.27 \pm 0.70	89.90 \pm 0.60	58.48 \pm 1.35	93.00 \pm 0.28	86.48 \pm 0.86	76.46 \pm 0.58
HRP(ours)	55.47\pm0.97	86.19\pm0.64	91.55\pm0.22	59.09\pm3.60	93.31 \pm 0.14	87.06\pm0.13	78.78\pm0.65
AsymLoRA	28.22 \pm 0.70	68.14 \pm 0.35	85.12 \pm 0.70	51.26 \pm 2.34	91.90 \pm 0.44	8.02 \pm 1.51	55.44 \pm 0.54
PiSSA	43.19 \pm 0.52	69.53 \pm 0.42	88.33 \pm 0.23	54.63 \pm 0.85	92.58 \pm 0.05	34.74 \pm 12.65	63.83 \pm 1.89
HRP(ours)	52.07\pm2.27	77.86\pm2.58	90.05\pm0.14	59.81\pm1.36	92.93\pm0.24	83.37\pm0.33	76.01\pm0.15

eters from pre-trained weights.

- Classic LoRA with different initialization methods (zero+random initialization is settled in RSI): 1) kaiming normal initialization, 2) orthogonal initialization (Zhu et al., 2024), 3) PiSSA (Meng et al., 2024): first r right singular vectors of W^{pre} , 4) LoRA-GA (Wang et al., 2024): initializing A and B with first $2r$ left and right singular vectors of gradient approximation, and 5) our proposed HRP with 200 steps preheating.
- Asymmetric LoRA (Zhu et al., 2024) with different initialization methods (zero+random initialization is settled in RSI): orthogonal initialization, PiSSA, and HRP.
- Other LoRA variants including: a) DoRA (Liu et al., 2024): with additional learnable magnitudes, b) rsLoRA (Kalajdziewski, 2023): with a scaling factor for stability, and c) AdaLoRA (Zhang et al., 2023): with dynamically adjusted rank allocation.

5.1. Experiments on NLU tasks

In NLU tasks, we fine-tune the T5-base model (Raffel et al., 2020) by AdamW (Loshchilov & Hutter, 2019) on a subset of GLUE (Wang, 2018) benchmark, including CoLA, MRPC, QNLI, RTE, SST-2, and STS-B. Performance is evaluated on the Matthews correlation coefficient for CoLA, Pearson correlation coefficient for STS-B, and accuracy for the remaining tasks.

During fine-tuning, we fixed the learning rate to 4×10^{-4} for all tasks and fine-tuned 5 epochs on the CoLA task while others for 2 epochs. Each experiment is conducted with 3 different random seeds (fixed seeds across different

methods), and both the average and standard deviation are reported. For all variants of LoRA, we inject LoRA blocks for all query and value sub-modules with low rank $r = 4$ and $\alpha = 2r$. For HRP, we set the preheating rank $R = 128$ with $S = 200$ steps in the same training dataset with the AdamW optimizer under a constant learning rate. We present more implication detail in Appendix B.1.

As demonstrated in Table 4, HRP yields remarkable improvements in classic LoRA’s performance, enabling it to surpass all other initialization methods and other variants while achieving results comparable to FPFT. When examining Asymmetric LoRA specifically, we observed that both orthogonal and PiSSA initialization schemas initially exhibited suboptimal performance under our experimental setting of low rank $r = 4$. However, the introduction of just a few steps of HRP dramatically transformed the effectiveness of these same updating schemas, elevating their performance to levels comparable with classic LoRA.

5.2. Experiments on NLG tasks

In NLG tasks, we fine-tune the Llama2-7B model (Touvron et al., 2023), Qwen2-7B model (Yang et al., 2024), and Falcon3-7B model (Team, 2024) by AdamW (Loshchilov & Hutter, 2019) on a 50K subset of MetaMathQA dataset (Yu et al., 2023) for 1 epoch. Then, we evaluate the fine-tuned models on the test set of GSM8K (Cobbe et al., 2021) and MATH (Hendrycks et al., 2021b).

During fine-tuning, we fix the learning rate to 5×10^{-5} and fix the same random seed in all baselines. For all variants of LoRA, we inject LoRA blocks for all query, key, value, attention output, and all fully connected weight matrices, with rank $r = 8$ and $\alpha = 2r$ in the main fine-tuning process.

Table 2. Results with LLMs on math reasoning tasks. **Blue bold** marked denotes the best result across different LoRA initialization, and **red bold** marked denotes the best result overall baseline.

	GSM8K				MATH			
	Llama2	Qwen2	Falcon3	Avg.	Llama2	Qwen2	Falcon3	Avg.
rsLoRA	43.75	74.07	79.08	65.63	6.76	30.28	37.88	24.97
DoRA	42.53	74.60	79.08	65.40	6.22	29.84	37.88	24.65
FPFT	43.75	71.72	79.68	65.05	6.34	31.00	38.06	25.13
LoRA(Gauss)	28.89	74.22	79.98	61.03	3.90	32.32	33.72	23.31
LoRA(Orth)	29.72	73.31	78.92	60.65	3.40	29.42	32.48	21.76
PiSSA	31.24	72.86	75.44	59.85	3.80	29.32	34.62	22.58
LoRA-GA	23.58	72.86	78.92	58.45	2.56	29.32	32.34	21.41
HRP(ours)	34.65	75.36	79.15	63.05	3.98	30.74	36.80	23.84
AsymLoRA	22.44	75.21	79.30	58.98	1.36	36.64	32.60	23.53
PiSSA	28.58	72.71	79.68	60.32	2.50	31.88	33.30	22.56
HRP(ours)	32.07	77.18	76.19	61.81	4.06	30.82	35.96	23.61

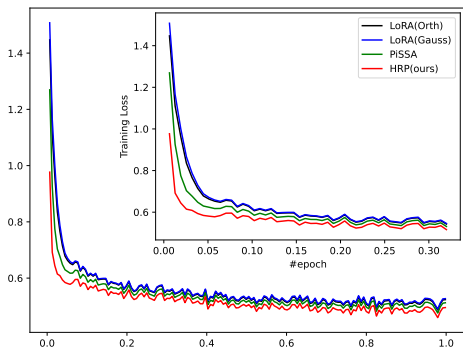


Figure 1. Training loss trajectories for Llama2-7B fine-tuned on MetaMathQA using different initialization strategies in classic LoRA. The inset figure (top right) highlights the loss dynamics during the first 500 optimization steps.

For HRP preheating stage, we set the preheating rank $R = 256$ with $S = 50$ steps in the same training dataset with the AdamW optimizer under a constant learning rate. Our model is fine-tuned using standard supervised learning fine-tuning schema for language modeling where the loss for the input prompt is set to zero. We present more implication detail in Appendix B.2.

We report the evaluated results in Table 5.2, which demonstrate the effectiveness of HRP across various large language models. Similar to results in NLU tasks, HRP yields substantial improvements for both classic LoRA and Asymmetric LoRA. It is crucial to note that HRP demonstrates more pronounced benefits when applied to the relatively under-trained Llama2 model, indicating that HRP’s effectiveness does not heavily depend on the performance of the pre-trained model.

Unlike results in NLU tasks, Asymmetric LoRA demonstrates sufficient expressiveness in these NLG tasks, despite having about half the trainable parameters compared to classic LoRA. HRP further enhances its fine-tuning capabilities with a few steps of fine-tuning steps, outperforming random orthogonal initialization and PiSSA initialization.

To provide deeper insights into the training dynamics, we present the loss curves of fine-tuning Llama2 in Figure 1. The visualization convincingly validates our theoretical analysis, demonstrating that HRP indeed achieves superior converged results compared with random initialization. Besides, the loss curves reveal that HRP also accelerates the convergence of classic LoRA, especially in the beginning stage of fine-tuning. Aside from Llama2, we also present the loss curves of fine-tuning other models in Appendix C.

6. Conclusion

In this paper, we first theoretically show the important role of LoRA initialization for convergence, where widely-used random initialization is likely to make Asymmetric LoRA converge to random low-rank results, rather than the best low-rank results and classic LoRA has similar properties.

Then, to address the problem, we propose HRP, an initialization algorithm that makes LoRA with low rank have better convergence properties (comparable with high-rank LoRA) while maintaining the small number of trainable parameters (thus holds generalization). HRP utilizes a few steps of high-rank LoRA optimization as the preheating stage and uses main singular vectors as initialization for low-rank LoRA.

We further evaluate the effectiveness of HRP through experiments on NLU and NLG tasks and various models, where HRP makes LoRA achieve better performance compared with other initialization strategies.

Impact Statement

This paper presents work whose goal is to advance the initialization of LoRA. A potential impact of this paper is guiding practitioners on more effective initialization for fine-tuning deep learning models using LoRA. After thorough consideration and analysis, it can be firmly stated that this research has no ethical aspects that could raise concerns.

References

- Achiam, J., Adler, S., Agarwal, S., Ahmad, L., Akkaya, I., Aleman, F. L., Almeida, D., Altenschmidt, J., Altman, S., Anadkat, S., et al. Gpt-4 technical report. *arXiv preprint arXiv:2303.08774*, 2023.
- Bałazy, K., Banaei, M., Aberer, K., and Tabor, J. Lora-xs: Low-rank adaptation with extremely small number of parameters. *arXiv preprint arXiv:2405.17604*, 2024.
- Biderman, D., Portes, J., Ortiz, J. J. G., Paul, M., Greengard, P., Jennings, C., King, D., Havens, S., Chiley, V., Frankle, J., et al. Lora learns less and forgets less. *arXiv preprint arXiv:2405.09673*, 2024.
- Bommasani, R., Hudson, D. A., Adeli, E., Altman, R., Arora, S., von Arx, S., Bernstein, M. S., Bohg, J., Bosse-lut, A., Brunskill, E., et al. On the opportunities and risks of foundation models. *arXiv preprint arXiv:2108.07258*, 2021.
- Büyükakyüz, K. Olora: Orthonormal low-rank adaptation of large language models. *arXiv preprint arXiv:2406.01775*, 2024.
- Chi, Y., Lu, Y. M., and Chen, Y. Nonconvex optimization meets low-rank matrix factorization: An overview. *IEEE Transactions on Signal Processing*, 67(20):5239–5269, 2019.
- Cobbe, K., Kosaraju, V., Bavarian, M., Chen, M., Jun, H., Kaiser, L., Plappert, M., Tworek, J., Hilton, J., Nakano, R., Hesse, C., and Schulman, J. Training verifiers to solve math word problems. *arXiv preprint arXiv:2110.14168*, 2021.
- Dauphin, Y. N. and Schoenholz, S. Metainit: Initializing learning by learning to initialize. *Advances in Neural Information Processing Systems*, 32, 2019.
- Eckart, C. and Young, G. The approximation of one matrix by another of lower rank. *Psychometrika*, 1(3):211–218, 1936.
- Filatov, N. and Kindulov, M. Low rank adaptation for stable domain adaptation of vision transformers. *Optical Memory and Neural Networks*, 32(Suppl 2):S277–S283, 2023.
- Fu, S., Chen, Y., Wang, Y., and Tao, D. On championing foundation models: From explainability to interpretability. *arXiv preprint arXiv:2410.11444*, 2024a.
- Fu, S., Zhang, S., Wang, Y., Tian, X., and Tao, D. Towards theoretical understandings of self-consuming generative models. *arXiv preprint arXiv:2402.11778*, 2024b.
- Glorot, X. and Bengio, Y. Understanding the difficulty of training deep feedforward neural networks. In *Proceedings of the thirteenth international conference on artificial intelligence and statistics*, pp. 249–256. JMLR Workshop and Conference Proceedings, 2010.
- Hayou, S., Ghosh, N., and Yu, B. The impact of initialization on lora finetuning dynamics. *arXiv preprint arXiv:2406.08447*, 2024a.
- Hayou, S., Ghosh, N., and Yu, B. Lora+: Efficient low rank adaptation of large models. *arXiv preprint arXiv:2402.12354*, 2024b.
- He, K., Zhang, X., Ren, S., and Sun, J. Delving deep into rectifiers: Surpassing human-level performance on imagenet classification. In *Proceedings of the IEEE international conference on computer vision*, pp. 1026–1034, 2015.
- Hendrycks, D., Burns, C., Kadavath, S., Arora, A., Basart, S., Tang, E., Song, D., and Steinhardt, J. Measuring mathematical problem solving with the math dataset. *arXiv preprint arXiv:2103.03874*, 2021a.
- Hendrycks, D., Burns, C., Kadavath, S., Arora, A., Basart, S., Tang, E., Song, D., and Steinhardt, J. Measuring mathematical problem solving with the math dataset. *arXiv preprint arXiv:2103.03874*, 2021b.
- Howard, R. The gronwall inequality. *lecture notes*, 1998.
- Hu, E. J., Shen, Y., Wallis, P., Allen-Zhu, Z., Li, Y., Wang, S., Wang, L., and Chen, W. Lora: Low-rank adaptation of large language models. *arXiv preprint arXiv:2106.09685*, 2021.
- Ji, Y., Liu, Y., Zhang, Z., Zhang, Z., Zhao, Y., Zhou, G., Zhang, X., Liu, X., and Zheng, X. Advlora: Adversarial low-rank adaptation of vision-language models. *arXiv preprint arXiv:2404.13425*, 2024.
- Kalajdziewski, D. A rank stabilization scaling factor for fine-tuning with lora. *arXiv preprint arXiv:2312.03732*, 2023.
- Kopiczko, D. J., Blankevoort, T., and Asano, Y. M. Vera: Vector-based random matrix adaptation. *arXiv preprint arXiv:2310.11454*, 2023.

- Kumar, A., Raghunathan, A., Jones, R., Ma, T., and Liang, P. Fine-tuning can distort pretrained features and underperform out-of-distribution. *arXiv preprint arXiv:2202.10054*, 2022.
- Li, B., Zhang, L., Mokhtari, A., and He, N. On the crucial role of initialization for matrix factorization. *arXiv preprint arXiv:2410.18965*, 2024.
- Liu, H., Tam, D., Muqeeth, M., Mohta, J., Huang, T., Bansal, M., and Raffel, C. A. Few-shot parameter-efficient fine-tuning is better and cheaper than in-context learning. *Advances in Neural Information Processing Systems*, 35: 1950–1965, 2022.
- Liu, S.-Y., Wang, C.-Y., Yin, H., Molchanov, P., Wang, Y.-C. F., Cheng, K.-T., and Chen, M.-H. Dora: Weight-decomposed low-rank adaptation. *arXiv preprint arXiv:2402.09353*, 2024.
- Loshchilov, I. and Hutter, F. Decoupled weight decay regularization, 2019. URL <https://arxiv.org/abs/1711.05101>.
- Malinovsky, G., Michieli, U., Hammoud, H. A. A. K., Ceritli, T., Elesedy, H., Ozay, M., and Richtárik, P. Randomized asymmetric chain of lora: The first meaningful theoretical framework for low-rank adaptation. *arXiv preprint arXiv:2410.08305*, 2024.
- Mao, Y., Ge, Y., Fan, Y., Xu, W., Mi, Y., Hu, Z., and Gao, Y. A survey on lora of large language models. *Frontiers of Computer Science*, 19(7):197605, 2025.
- Meng, F., Wang, Z., and Zhang, M. Pissa: Principal singular values and singular vectors adaptation of large language models. *arXiv preprint arXiv:2404.02948*, 2024.
- Min, H., Tarmoun, S., Vidal, R., and Mallada, E. On the explicit role of initialization on the convergence and implicit bias of overparametrized linear networks. In *International Conference on Machine Learning*, pp. 7760–7768. PMLR, 2021.
- Mishkin, D. and Matas, J. All you need is a good init. *arXiv preprint arXiv:1511.06422*, 2015.
- Patel, V., Zhang, S., and Tian, B. Global convergence and stability of stochastic gradient descent. *Advances in Neural Information Processing Systems*, 35:36014–36025, 2022.
- Ponkshe, K., Singhal, R., Gorbunov, E., Tumanov, A., Horvath, S., and Vepakomma, P. Initialization using update approximation is a silver bullet for extremely efficient low-rank fine-tuning. *arXiv preprint arXiv:2411.19557*, 2024.
- Raffel, C., Shazeer, N., Roberts, A., Lee, K., Narang, S., Matena, M., Zhou, Y., Li, W., and Liu, P. J. Exploring the limits of transfer learning with a unified text-to-text transformer. *Journal of Machine Learning Research*, 21(140):1–67, 2020. URL <http://jmlr.org/papers/v21/20-074.html>.
- Renduchintala, A., Konuk, T., and Kuchaiev, O. Tied-lora: Enhancing parameter efficiency of lora with weight tying. *arXiv preprint arXiv:2311.09578*, 2023.
- Saxe, A. M., McClelland, J. L., and Ganguli, S. Exact solutions to the nonlinear dynamics of learning in deep linear neural networks. *arXiv preprint arXiv:1312.6120*, 2013.
- Song, Y., Zhao, J., Harris, I. G., and Jyothi, S. A. Sharelora: Parameter efficient and robust large language model fine-tuning via shared low-rank adaptation. *arXiv preprint arXiv:2406.10785*, 2024.
- Tarmoun, S., Franca, G., Haeffele, B. D., and Vidal, R. Understanding the dynamics of gradient flow in overparameterized linear models. In *International Conference on Machine Learning*, pp. 10153–10161. PMLR, 2021.
- Team, T. The falcon 3 family of open models, December 2024.
- Touvron, H., Martin, L., Stone, K., Albert, P., Almahairi, A., Babaei, Y., Bashlykov, N., Batra, S., Bhargava, P., Bhosale, S., et al. Llama 2: Open foundation and fine-tuned chat models. *arXiv preprint arXiv:2307.09288*, 2023.
- Wang, A. Glue: A multi-task benchmark and analysis platform for natural language understanding. *arXiv preprint arXiv:1804.07461*, 2018.
- Wang, H., Agarwal, S., and Papailiopoulos, D. Pufferfish: Communication-efficient models at no extra cost. *Proceedings of Machine Learning and Systems*, 3:365–386, 2021.
- Wang, H., Agarwal, S., Tanaka, Y., Xing, E., Papailiopoulos, D., et al. Cuttlefish: Low-rank model training without all the tuning. *Proceedings of Machine Learning and Systems*, 5:578–605, 2023.
- Wang, S., Yu, L., and Li, J. Lora-ga: Low-rank adaptation with gradient approximation. *arXiv preprint arXiv:2407.05000*, 2024.
- Wind, J. S. Asymmetric matrix sensing by gradient descent with small random initialization. *arXiv preprint arXiv:2309.01796*, 2023.

- Xia, W., Qin, C., and Hazan, E. Chain of lora: Efficient fine-tuning of language models via residual learning. *arXiv preprint arXiv:2401.04151*, 2024.
- Yang, A., Yang, B., Hui, B., Zheng, B., Yu, B., Zhou, C., Li, C., Li, C., Liu, D., Huang, F., Dong, G., Wei, H., Lin, H., Tang, J., Wang, J., Yang, J., Tu, J., Zhang, J., Ma, J., Xu, J., Zhou, J., Bai, J., He, J., Lin, J., Dang, K., Lu, K., Chen, K., Yang, K., Li, M., Xue, M., Ni, N., Zhang, P., Wang, P., Peng, R., Men, R., Gao, R., Lin, R., Wang, S., Bai, S., Tan, S., Zhu, T., Li, T., Liu, T., Ge, W., Deng, X., Zhou, X., Ren, X., Zhang, X., Wei, X., Ren, X., Fan, Y., Yao, Y., Zhang, Y., Wan, Y., Chu, Y., Liu, Y., Cui, Z., Zhang, Z., and Fan, Z. Qwen2 technical report. *arXiv preprint arXiv:2407.10671*, 2024.
- Yang, Y., Wang, H., Yuan, H., and Lin, Z. Towards theoretically inspired neural initialization optimization. *Advances in Neural Information Processing Systems*, 35: 18983–18995, 2022.
- Ye, T. and Du, S. S. Global convergence of gradient descent for asymmetric low-rank matrix factorization. *Advances in Neural Information Processing Systems*, 34: 1429–1439, 2021.
- Yu, L., Jiang, W., Shi, H., Yu, J., Liu, Z., Zhang, Y., Kwok, J. T., Li, Z., Weller, A., and Liu, W. Metamath: Bootstrap your own mathematical questions for large language models. *arXiv preprint arXiv:2309.12284*, 2023.
- Zeng, Y. and Lee, K. The expressive power of low-rank adaptation. *arXiv preprint arXiv:2310.17513*, 2023.
- Zhang, Q., Chen, M., Bukharin, A., Karampatziakis, N., He, P., Cheng, Y., Chen, W., and Zhao, T. Adalora: Adaptive budget allocation for parameter-efficient fine-tuning. *arXiv preprint arXiv:2303.10512*, 2023.
- Zhu, C., Ni, R., Xu, Z., Kong, K., Huang, W. R., and Goldstein, T. Gradinit: Learning to initialize neural networks for stable and efficient training. *Advances in Neural Information Processing Systems*, 34:16410–16422, 2021.
- Zhu, J., Greenewald, K., Nadjahi, K., Borde, H. S. d. O., Gabrielsson, R. B., Choshen, L., Ghassemi, M., Yurochkin, M., and Solomon, J. Asymmetry in low-rank adapters of foundation models. *arXiv preprint arXiv:2402.16842*, 2024.

A. Proof for Theorems

In this section, we present the proof for the theorems above. We begin with some useful lemmas and their proofs.

Lemma A.1. *Gradient flow 2 under problem 3 with $\eta_A = \eta, \eta_B = 0$, X_t has the following closed form:*

$$X_t = [I - e^{-\eta Z_0 t}] M, \quad (5)$$

with $\eta_A = 0, \eta_B = \eta$, X_t has the following closed form:

$$X_t = M [I - e^{-\eta Y_0 t}] \quad (6)$$

where e^A denotes exponential operation on matrix.

Proof. When $\eta_A = \eta, \eta_B = 0$, the gradient flow becomes

$$\begin{cases} \dot{X}_t = -\eta Z_t G_t, \\ \dot{Y}_t = -\eta X_t^\top G_t - \eta G_t^\top X_t, \\ \dot{Z}_t = 0, \end{cases} \quad (7)$$

which means $Z_t \equiv Z_0$ for all t , and $\dot{X}_t = -\eta Z_0 (X_t - M)$. Then X_t has analytic solution

$$X_t = [I - e^{-\eta Z_0 t}] M + X_0 = [I - e^{-\eta Z_0 t}] M. \quad (8)$$

When $\eta_A = 0, \eta_B = \eta$, the gradient flow becomes

$$\begin{cases} \dot{X}_t = -\eta G_t Y_t, \\ \dot{Y}_t = O_{a \times a} \\ \dot{Z}_t = -\eta X_t G_t^\top - \eta G_t X_t^\top, \end{cases} \quad (9)$$

which means $Y_t \equiv Y_0$ for all t , and $\dot{X}_t = -\eta (X_t - M) Y_0$. Then X_t has analytic solution

$$X_t = M [I - e^{-\eta Y_0 t}] + X_0 = M [I - e^{-\eta Y_0 t}]. \quad (10)$$

□

Lemma A.2. *For any matrix $A \in \mathbb{R}^{d_1 \times d_2}$ and any orthogonal matrix $U \in \mathbb{R}^{d_1 \times d_1}$, and $r \leq d_2$, for*

$$X = U \begin{pmatrix} I_r & \\ & O_{(d_1-r) \times (d_1-r)} \end{pmatrix} U^\top M, \quad (11)$$

we have

$$\|M - X\|_F^2 = \|M\|_F^2 - \|X\|_F^2. \quad (12)$$

Proof. We have

$$\|M\|_F^2 = \|X\|_F^2 + \|M - X\|_F^2 + 2 \text{Trace}(X^\top (M - X)). \quad (13)$$

Then it is sufficient to prove $\text{Trace}(X^\top (M - X)) = 0$. In fact, we have

$$\text{Trace}(X^\top (M - X)) = \text{Trace} \left(\left[U \begin{pmatrix} I_r & \\ & O_{(d_1-r) \times (d_1-r)} \end{pmatrix} U^\top M \right]^\top \left[M - U \begin{pmatrix} I_r & \\ & O_{(d_1-r) \times (d_1-r)} \end{pmatrix} U^\top M \right] \right) \quad (14)$$

$$= \text{Trace} \left(\left[U \begin{pmatrix} I_r & \\ & O_{(d_1-r) \times (d_1-r)} \end{pmatrix} U^\top M \right]^\top \left[U \begin{pmatrix} O_{r \times r} & \\ & I_{d_1-r} \end{pmatrix} U^\top M \right] \right) \quad (15)$$

$$= \text{Trace} \left(M^\top U \begin{pmatrix} I_r & \\ & O_{(d_1-r) \times (d_1-r)} \end{pmatrix} U^\top U \begin{pmatrix} O_{r \times r} & \\ & I_{d_1-r} \end{pmatrix} U^\top M \right) \quad (16)$$

$$= \text{Trace}(O_{d_1 \times d_1}) = 0. \quad (17)$$

□

Theorem A.3 (Gronwall's Theorem). For $x_t \geq 0$ and inequality

$$dx_t \leq [ax_t + bt]dt, \quad x_0 = 0, \quad (18)$$

we have

$$x_t = O(bt^2) \quad (19)$$

Proof. Consider $x_t e^{-at} \geq 0$ and

$$d[x_t e^{-at}] \leq e^{-at}[ax_t + bt]dt - ax_t e^{-at} dt = bte^{-at} dt \quad (20)$$

thus

$$x_t e^{-at} \leq x_0 + \int_0^t bse^{-as} ds = \frac{b}{a^2}[-(1+at)e^{-at} + 1] \quad (21)$$

$$x_t \leq \frac{b}{a^2}[e^{at} - at - 1] = O(bt^2) \quad (22)$$

□

Remark A.4. Theorem A.3 presents a simplified version of the Gronwall inequality (Howard, 1998). In the original inequality, the terms ax_t and bt have more complex forms, and the result is not expressed in big-O notation. We use this simplified version to establish bounds on the difference between Asymmetric LoRA and classical LoRA in the proof that follows.

A.1. Proof for Theorem 3.1

Theorem A.5 (Restatement of theorem 3.1). For Asymmetric LoRA under problem 3 with Gaussian initialization and orthogonal initialization in LSI and RSI in zero+random schema, we have:

$$\mathbb{E}_{LSI} \left[\mathcal{L}(\lim_{t \rightarrow \infty} X_t) \right] = \frac{b-r}{2b} \sum_{i=1}^{\min\{a,b\}} \sigma_i(M)^2,$$

$$\mathbb{E}_{RSI} \left[\mathcal{L}(\lim_{t \rightarrow \infty} X_t) \right] = \frac{a-r}{2a} \sum_{i=1}^{\min\{a,b\}} \sigma_i(M)^2,$$

where \mathbb{E} represents the expectation for randomness in initialization.

Proof. For LSI, $\eta_A = \eta$, $\eta_B = 0$, according to Lemma A.1 we have

$$X_t = [I - e^{-\eta Z_0 t}] M = [I - e^{-\eta B_0 B_0^\top t}] M. \quad (23)$$

For the SVD decomposition of $B_0 = U_B \Sigma_B V_B^\top$, we have $Z_0 = U_B (\Sigma_B)^2 U_B^\top$ where Σ_B is a diagonal matrix with only first r elements non-zero. Then, consider $t \rightarrow \infty$, we have

$$\lim_{t \rightarrow \infty} X_t = \lim_{t \rightarrow \infty} [[I - e^{-\eta Z_0 t}] M] \quad (24)$$

$$= [I - \lim_{t \rightarrow \infty} e^{-\eta Z_0 t}] M \quad (25)$$

$$= U_B \left[I - \lim_{t \rightarrow \infty} e^{-\eta \Sigma_B^2 t} \right] U_B^\top M = U_B \begin{pmatrix} I_r & \\ & O_{b-r} \end{pmatrix} U_B^\top M. \quad (26)$$

Gaussian initialization and orthogonal initialization share the same probability for the same U_B , thus their properties at converged results are the same. The loss of the converged result satisfies:

$$\mathcal{L}(\lim_{t \rightarrow \infty} X_t) = \|\lim_{t \rightarrow \infty} X_t - M\|_F^2 \quad (27)$$

$$= \frac{1}{2} \left\| U_B \begin{pmatrix} I_r & \\ & O_{b-r} \end{pmatrix} U_B^\top M - M \right\|_F^2 \quad (28)$$

$$= \frac{1}{2} \left\| U_B \begin{pmatrix} O_r & \\ & I_{b-r} \end{pmatrix} U_B^\top M \right\|_F^2 \quad (29)$$

$$= \frac{1}{2} \left\| \begin{pmatrix} O_r & \\ & I_{b-r} \end{pmatrix} U_B^\top M \right\|_F^2 \quad (30)$$

$$= \frac{1}{2} \sum_{i=r}^b \|U_{B,i}^\top M\|_F^2, \quad (31)$$

where $U_{B,i}^\top$ is the i -th column of U_B thus the i -th row of U_B^\top and orthogonal with each other. For any orthogonal matrix U , consider $U^{(i)} = [U_{[:,i]}, U_{[:,i]}]$. Due to Gaussian initialization of B , the p.d.f at $U_B = U^{(i)}$ is the same as p.d.f at $U_B = U^{(j)}$ for all i, j . Thus, we have

$$\mathbb{E}_B \mathcal{L}(\lim_{t \rightarrow \infty} X_t) = \mathbb{E}_B \frac{1}{2} \sum_{i=r}^b \|U_{B,i}^\top M\|_F^2, \quad (32)$$

$$= \mathbb{E}_U \frac{1}{2b} \sum_{j=1}^b \sum_{i=r}^b \|U_{B,i}^\top M\|_F^2 \Bigg|_{U_B=U^{(j)}}, \quad (33)$$

$$= \frac{1}{2b} \sum_{i=r}^b \mathbb{E}_U \sum_{j=1}^b \|U_j^\top M\|_F^2, \quad (34)$$

$$= \frac{1}{2b} \sum_{i=r}^b \mathbb{E}_U \|U^\top M\|_F^2, \quad (35)$$

$$= \frac{1}{2b} \sum_{i=r}^b \|M\|_F^2 = \frac{b-r}{2b} \sum_{i=1}^{\min\{a,b\}} \sigma_i(M)^2. \quad (36)$$

For RSI in matrix sensing, it is equivalent to LSI with X^\top approximating M^\top , thus for RSI we have

$$\mathbb{E}_{RSI} \left[\mathcal{L}(\lim_{t \rightarrow \infty} X_t) \right] = \frac{a-r}{2a} \sum_{i=1}^{\min\{a,b\}} \sigma_i(M)^2 \quad (37)$$

□

A.2. Proof for Theorem 3.2

Theorem A.6 (Restatement of theorem 3.2). *For Asymmetric LoRA under problem 3 with LSI or RSI, we have*

$$\Pr \left[\mathcal{L}(\lim_{t \rightarrow \infty} X_t) = \mathcal{L}^* \right] = 0,$$

where \Pr represents the probability for initialization.

Proof. According to 26 and Eckart-Young Theorem (Eckart & Young, 1936), we have for LSI:

$$\Pr \left[\mathcal{L}(\lim_{t \rightarrow \infty} X_t) = \mathcal{L}^* \right] = \Pr \left[\forall i \in [r] : U_B \begin{pmatrix} I_r & \\ & O_{b-r} \end{pmatrix} U_B^\top M V_{M,i} = \sigma_i(M) U_{M,i} \right] \quad (38)$$

$$= \Pr \left[\forall i \in [r] : U_B \begin{pmatrix} I_r & \\ & O_{b-r} \end{pmatrix} U_B^\top U_{M,i} = U_{M,i} \right] \quad (39)$$

$$= \Pr \left[\forall i > r, j < r : (U_B^\top U_M)[i, j] = 0 \right] \quad (40)$$

Since U_B is random and independent from U_M , it is zero-probability for making left-down $(b-r) \times r$ matrix zero.

For RSI in matrix sensing, it is equivalent to LSI with X^\top approximating M^\top , thus for both LSI and RSI, we have

$$\Pr \left[\mathcal{L}(\lim_{t \rightarrow \infty} X_t) = \mathcal{L}^* \right] = 0,$$

□

A.3. Proof for Theorem 3.3

Theorem A.7 (Restatement of theorem 3.3). *For problem 3, if there exists $i \leq r$ making A, B with $A^\top v_i = O_a, B^\top u_i = O_b$. Then classic LoRA under LSI with $A_0 = A, B_0 = O_{b \times r}$ or RSI with $A_0 = O_{a \times r}, B_0 = B$, we have for any t :*

$$X_t v_i = O_b, \quad \text{and} \quad X_t^\top u_i = O_a,$$

resulting in

$$\mathcal{L}(X_t) - \mathcal{L}^* \geq \frac{1}{2} [\sigma_i(M)^2 - \sigma_{r+1}(M)^2] > 0,$$

where $M = U_M \Sigma_M V_M^\top$ is the SVD decomposition of M .

Proof. LSI with $A_0 = A, B_0 = O_{b \times r}$ means that initialization of X, Y, Z satisfies

$$X_0 = O_{a \times b}, \quad Y_0 = AA^\top, \quad Z_0 = O_{b \times b}, \quad (41)$$

indicating for $t = 0$, we have:

$$X_t v_i = O_b, \quad Y_t v_i = O_a, \quad X_t^\top u_i = O_a, \quad Z_t^\top u_i = O_b. \quad (42)$$

RSI with $A_0 = O_{a \times r}, B_0 = B$ means that initialization of X, Y, Z satisfies

$$X_0 = O_{b \times a}, \quad Y_0 = O_{a \times a}, \quad Z_0 = BB^\top, \quad (43)$$

which also indicates 42 true for $t = 0$. We then prove 42 true for all $t > 0$ to prove Theorem 3.3. According to induction, it is sufficient to prove each gradient to t in 42 to be zero for all t . In fact, we have

$$\frac{d(X_t v_i)}{dt} = \dot{X}_t v_i = -\eta Z_t (X_t - M) v_i - \eta (X_t - M) Y_t v_i = \eta Z_t M v_i = \eta \sigma_i(M) Z_t u_i = O_b, \quad (44)$$

$$\frac{d(Y_t v_i)}{dt} = \dot{Y}_t v_i = -\eta X_t^\top (X_t - M) v_i - \eta (X_t - M)^\top X_t v_i = \eta X_t^\top M v_i = \eta \sigma_i(M) X_t^\top u_i = O_a, \quad (45)$$

$$\frac{d(X_t^\top u_i)}{dt} = \dot{X}_t^\top u_i = -\eta [Z_t (X_t - M)]^\top u_i - \eta [(X_t - M) Y_t]^\top u_i = \eta Y_t M^\top u_i = \eta \sigma_i(M) Y_t v_i = O_a, \quad (46)$$

$$\frac{d(Z_t u_i)}{dt} = \dot{Z}_t u_i = -\eta X_t (X_t - M)^\top u_i - \eta (X_t - M) X_t^\top u_i = \eta X_t M^\top u_i = \eta \sigma_i(M) X_t v_i = O_b. \quad (47)$$

This means that the composition $\sigma_i(M) u_i v_i^\top$ will not emerge from X_t as t grows up. However, the best low-rank approximation of M requires $\sigma_i(M) u_i v_i^\top$ to be included, which makes the optimization never converge to the best low-rank

result. For loss, consider $M' = M - \sigma_i(M)u_i v_i^\top$, we have

$$\mathcal{L}(X_t) = \frac{1}{2} \|X - M\|_F^2 = \frac{1}{2} \text{Trace}((X - M' - \sigma_i(M)u_i v_i^\top)(X - M' - \sigma_i(M)u_i v_i^\top)^\top) \quad (48)$$

$$= \frac{1}{2} \|X - M'\|_F^2 + \frac{1}{2} \|\sigma_i(M)u_i v_i^\top\|_F^2 \quad (49)$$

$$\geq \frac{1}{2} \sum_{j=r+2}^{\min\{a,b\}} \sigma_j(M)^2 + \frac{1}{2} \sigma_i(M)^2 \quad (50)$$

$$= \mathcal{L}^* + \frac{1}{2} [\sigma_i(M)^2 - \sigma_{r+1}(M)^2] \quad (51)$$

□

A.4. Proof for Theorem 3.4

Theorem A.8 (Restatement of theorem 3.4). *Assume $\{X_s\}_{0 \leq s \leq t}$ is bounded by R and the computed gradient $X_t \rightarrow G_t$ is Lipschitz in the Frobenius norm (same gradient calculator for classic LoRA and Asymmetric LoRA), then the difference between the dynamic of Asymmetric LoRA (\tilde{X}_t) and the dynamic of classic LoRA (X_t) is upper bounded by*

$$\|X_t - \tilde{X}_t\|_F \leq O(\eta R^3 t^2), \quad (52)$$

when they have the same initialization in LSI or RSI.

Proof. We use Gronwall's Theorem A.3 to bound the difference $\|X_t - \tilde{X}_t\|_F$. Recall X_t and \tilde{X}_t follows the differential equations:

$$\begin{cases} \dot{X}_t = -\eta_A Z_t G_t - \eta_B G_t Y_t, \\ \dot{Y}_t = -\eta_A X_t^\top G_t - \eta_A G_t^\top X_t, \\ \dot{Z}_t = -\eta_B X_t G_t^\top - \eta_B G_t X_t^\top, \end{cases} \quad \text{and} \quad \begin{cases} \dot{\tilde{X}}_t = -\eta_A Z_0 \tilde{G}_t - \eta_B \tilde{G}_t Y_0. \end{cases} \quad (53)$$

Taking the assumption $X_t \rightarrow G_t$ to be L -Lipschitz and bounded X_t , we have

$$\|G_t\|_F \leq LR + \|G_0\|_F, \quad \text{and} \quad \|\tilde{G}_t - G_t\|_F \leq L \|X_t - \tilde{X}_t\|_F. \quad (54)$$

Then the difference of Y_t and Z_t can be bounded through

$$\|Y_t - Y_0\|_F \leq \int_0^t \|dY_s\|_F \leq \eta \int_0^t 2 \|X_t\|_F \|G_t\|_F dt \leq 2\eta R (\|G_0\|_F + LR)t, \quad (55)$$

$$\|Z_t - Z_0\|_F \leq \int_0^t \|dZ_s\|_F \leq \eta \int_0^t 2 \|X_t\|_F \|G_t\|_F dt \leq 2\eta R (\|G_0\|_F + LR)t. \quad (56)$$

We then calculate the difference between $\dot{\tilde{X}}_t$ and \dot{X}_t :

$$\dot{X}_t - \dot{\tilde{X}}_t = -\eta Z_t G_t - \eta G_t Y_t - [-\eta Z_0 \tilde{G}_t - \eta \tilde{G}_t Y_0] \quad (57)$$

$$= -\eta (Z_t - Z_0) G_t - \eta Z_0 (G_t - \tilde{G}_t) - \eta G_t (Y_t - Y_0) - \eta (G_t - \tilde{G}_t) Y_0. \quad (58)$$

Taking Frobenius norm of LHS and RHS we have:

$$\frac{d \|X_t - \tilde{X}_t\|_F}{dt} \leq \left\| \frac{d[X_t - \tilde{X}_t]}{dt} \right\|_F \quad (59)$$

$$\leq \left\| -\eta (Z_t - Z_0) G_t - \eta Z_0 (G_t - \tilde{G}_t) - \eta G_t (Y_t - Y_0) - \eta (G_t - \tilde{G}_t) Y_0 \right\|_F \quad (60)$$

$$\leq \eta (\|Z_t - Z_0\|_F \|G_t\|_F + \eta \|Z_0 (G_t - \tilde{G}_t)\|_F + \eta \|G_t (Y_t - Y_0)\|_F + \eta \|(G_t - \tilde{G}_t) Y_0\|_F) \quad (61)$$

$$\leq \eta (\|Z_t - Z_0\|_F \|G_t\|_F + \eta \|Z_0\|_F \|G_t - \tilde{G}_t\|_F + \eta \|G_t\|_F \|Y_t - Y_0\|_F + \eta \|G_t - \tilde{G}_t\|_F \|Y_0\|_F) \quad (62)$$

$$\leq \eta \left[\|G_t\|_F (\|Y_t - Y_0\|_F + \|Z_t - Z_0\|_F) + (\|Z_0\|_F + \|Y_0\|_F) \|G_t - \tilde{G}_t\|_F \right] \quad (63)$$

$$\leq \eta \left[4R (\|G_0\|_F + LR)^2 t + L (\|Z_0\|_F + \|Y_0\|_F) \|X_t - \tilde{X}_t\|_F \right]. \quad (64)$$

Thus according to Gronwall theorem A.3, we have

$$\|X_t - \tilde{X}_t\|_F \leq O(4R(\|G_0\| + LR)^2 t^2) = O(\eta R^3 t^2). \quad (65)$$

□

A.5. Proof for Theorem 3.5

Theorem A.9 (Restatement of theorem 3.5). *For Asymmetric LoRA under problem 3 in RSI with $A_0 = V_M[:, : r]$, $B_0 = O_{b \times r}$ or LSI with $A_0 = O_{a \times r}$, $B_0 = U_M[:, : r]$, we have*

$$\mathcal{L}(X_t) - \mathcal{L}^* = O(\exp\{-\eta t\}),$$

where $M = U_M \Sigma_M V_M^\top$ is the SVD decomposition of M .

Proof. According to Lemma A.1, with LSI and initialization $A_0 = V_M[:, : r]$, $B_0 = O_{b \times r}$, we have

$$X_t = M[I - e^{-\eta A_0 A_0^\top} t] = (1 - e^{-\eta t}) M V_M \begin{pmatrix} I_r & \\ & O_{(a-r) \times (a-r)} \end{pmatrix} V_M^\top, \quad (66)$$

which has loss

$$\mathcal{L}(X_t) = \frac{1}{2} \|X_t - M\|_F^2 \quad (67)$$

$$= \frac{1}{2} \left\| M - (1 - e^{-\eta t}) M V_M \begin{pmatrix} I_r & \\ & O_{(a-r) \times (a-r)} \end{pmatrix} V_M^\top \right\|_F^2 \quad (68)$$

$$= \frac{1}{2} \left\| U_M \Sigma_M V_M^\top - (1 - e^{-\eta t}) U_M \Sigma_M \begin{pmatrix} I_r & \\ & O_{(a-r) \times (a-r)} \end{pmatrix} V_M^\top \right\|_F^2 \quad (69)$$

$$= \frac{1}{2} \left\| \Sigma_M - (1 - e^{-\eta t}) \Sigma_M \begin{pmatrix} I_r & \\ & O_{(a-r) \times (a-r)} \end{pmatrix} \right\|_F^2 \quad (70)$$

$$= \frac{1}{2} \left\| \Sigma_M \begin{pmatrix} e^{-\eta t} I_r & \\ & I_{a-r} \end{pmatrix} \right\|_F^2 \quad (71)$$

$$= \frac{1}{2} e^{-\eta t} \sum_{i=1}^r \sigma_i(M)^2 + \frac{1}{2} \sum_{i=r+1}^{\min\{a,b\}} \sigma_i(M)^2 \quad (72)$$

$$= O(\exp\{-\eta t\}) + \mathcal{L}^*. \quad (73)$$

□

A.6. Proof for Theorem 3.6

Theorem A.10 (Restatement of theorem 3.6). *For classic LoRA under problem 3 in RSI with $A_0 = V_M[:, : r]$, $B_0 = O_{b \times r}$ or LSI with $A_0 = O_{a \times r}$, $B_0 = U_M[:, : r]$, we have*

$$\mathcal{L}(X_t) - \mathcal{L}^* = O(\exp\{-(1 + k\sigma_r(M))\eta t\}),$$

where $M = U_M \Sigma_M V_M^\top$ is the SVD decomposition of M and $k = \frac{\sqrt{1+4\sigma_1(M)}-1}{\sigma_1(M)} > 0$.

Proof. We consider

$$\hat{X}_t := U^\top X_t V, \quad \hat{Y}_t := V^\top Y_t V, \quad \hat{Z}_t := U^\top Z_t U, \quad (74)$$

and first prove

$$\forall r, \hat{X}_t, \hat{Y}_t, \hat{Z}_t \text{ are diagonal matrices with only the first } r \text{ elements non-zero.} \quad (75)$$

If initialized with $A_0 = V_{:,r}, B_0 = O_{b \times r}$, then we have

$$\hat{X}_t := U^\top X_0 V = O_{b \times a}, \quad \hat{Y}_t := V^\top Y_0 V = \begin{pmatrix} I_r & \\ & O_{a-r} \end{pmatrix}, \quad \hat{Z}_t := U^\top Z_0 U = O_{b \times b}. \quad (76)$$

If initialized with $A_0 = O_{a \times r}, B_0 = U_{:,r}$, then we have

$$\hat{X}_t := U^\top X_0 V = O_{b \times a}, \quad \hat{Y}_t := V^\top Y_0 V = O_{a \times a}, \quad \hat{Z}_t := U^\top Z_0 U = \begin{pmatrix} I_r & \\ & O_{b-r} \end{pmatrix}. \quad (77)$$

Thus, claim 75 is true for $t = 0$. If it is true for t , then their gradient satisfies

$$\dot{\hat{X}}_t = U^\top [-\eta Z_t (X_t - M) - \eta (X_t - M) Y_t] V = -\eta \hat{Z}_t (\hat{X}_t - \Sigma) - \eta (\hat{X}_t - \Sigma) \hat{Y}_t, \quad (78)$$

$$\dot{\hat{Y}}_t = V^\top [-\eta X_t^\top (X_t - M) - \eta (X_t - M)^\top X_t] V = -\eta \hat{X}_t^\top (\hat{X}_t - \Sigma) - \eta (\hat{X}_t - \Sigma)^\top \hat{X}_t, \quad (79)$$

$$\dot{\hat{Z}}_t = U^\top [-\eta X_t (X_t - M)^\top - \eta (X_t - M) X_t^\top] U = -\eta \hat{X}_t (\hat{X}_t - \Sigma)^\top - \eta (\hat{X}_t - \Sigma) \hat{X}_t^\top, \quad (80)$$

which are all diagonal matrices with only the first r elements non-zero. Thus, claim 75 is true for all t . We denote the diagonal elements for $\hat{X}_t, \hat{Y}_t, \hat{Z}_t$ are $x_{t,i}, y_{t,i}, z_{t,i}$. Then for each i , we have

$$x_{t,i} = -\eta z_{t,i} (x_{t,i} - \sigma_i(M)) - \eta (x_{t,i} - \sigma_i(M)) y_{t,i} = -\eta (y_{t,i} + z_{t,i}) (x_{t,i} - \sigma_i(M)), \quad (81)$$

$$y_{t,i} = z_{t,i} = -\eta x_{t,i} (x_{t,i} - \sigma_i(M)) - \eta (x_{t,i} - \sigma_i(M)) x_{t,i} = -2\eta x_{t,i} (x_{t,i} - \sigma_i(M)), \quad (82)$$

and they are independent with other $j \neq i$. Consider

$$d[(y_{t,i} + z_{t,i})^2] = -4\eta (y_{t,i} + z_{t,i}) x_{t,i} (x_{t,i} - \sigma_i(M)) \quad (83)$$

$$= -4\eta x_{t,i} (y_{t,i} + z_{t,i}) (x_{t,i} - \sigma_i(M)) = 4d[x_{t,i}^2], \quad (84)$$

resulting in

$$y_{t,i} + z_{t,i} = \sqrt{(y_{0,i} + z_{0,i})^2 + 4x_{t,i}^2 - 4x_{0,i}^2} = \sqrt{1 + 4x_{t,i}^2}. \quad (85)$$

So, the dynamic of $x_{t,i}$ is

$$x_{t,i} = -\eta (y_{t,i} + z_{t,i}) (x_{t,i} - \sigma_i(M)) = -\eta \sqrt{1 + 4x_{t,i}^2} (x_{t,i} - \sigma_i(M)). \quad (86)$$

This means $0 \leq x_{t,i} \leq \sigma_i(M) \leq \sigma_1(M)$ and $x_{t,i}$ are monotonically increasing with respect to t . Due to the convex property of $\sqrt{1 + 4x^2}$, we have for $k = \frac{\sqrt{1 + 4\sigma_1(M)^2} - 1}{\sigma_1(M)}$:

$$\sqrt{1 + 4x_{t,i}^2} \geq 1 + kx_{t,i} \quad (87)$$

$$x_{t,i} \geq -\eta [1 + kx_{t,i}] (x_{t,i} - \sigma_i(M)) \quad (88)$$

Consider another flow

$$\dot{x}_{t,i} = -\eta [1 + kx_{t,i}] (x_{t,i} - \sigma_i(M)), \quad x_{0,i} = x_{0,i} = 0, \quad (89)$$

we have $x_{t,i} \leq x_{t,i} \leq \sigma_i(M)$, and $(\sigma_i(M) - x_{t,i})^2 = O(e^{-(1+k\sigma_i(M))\eta t})$. So, for X_t , we have

$$\mathcal{L}(X_t) - \mathcal{L}^* = \|U \hat{X}_t V^\top - M\|_F^2 - \mathcal{L}^* \quad (90)$$

$$= \|\hat{X}_t - \Sigma\|_F^2 - \mathcal{L}^* \quad (91)$$

$$= \sum_{i=1}^r (\sigma_i(M) - x_{t,i})^2 \quad (92)$$

$$\leq \sum_{i=1}^r (\sigma_i(M) - x_{0,i})^2 \quad (93)$$

$$= \sum_{i=1}^r O(\exp\{-(1+k\sigma_i(M))\eta t\}) \quad (94)$$

$$\leq O(\exp\{-(1+k\sigma_r(M))\eta t\}) \quad (95)$$

□

A.7. Proof for Theorem 4.1

Theorem A.11 (Restatement of theorem 4.1). *For HRP initialized Asymmetric LoRA with one preheating step and the same updating rules (LSI preheating with LSI fine-tuning or RSI preheating with RSI fine-tuning) under problem 3, if $\text{rank}(M) \leq r$ we have*

$$\begin{aligned}\mathbb{E}_{LSI} \left[\mathcal{L}(\lim_{t \rightarrow \infty} X_t) \right] &= \frac{b-R}{2b} \sum_{i=1}^r \sigma_i(M)^2, \\ \mathbb{E}_{RSI} \left[\mathcal{L}(\lim_{t \rightarrow \infty} X_t) \right] &= \frac{a-R}{2a} \sum_{i=1}^r \sigma_i(M)^2,\end{aligned}$$

where R is the rank at the preheating stage while r is the rank at the real optimizing stage.

Proof. According to Theorem 26, for LSI we have

$$\hat{X}_t = \left[I - e^{-\eta \hat{Z}_0 t} \right] M = (1 - e^{-\eta t}) U_B \begin{pmatrix} I_r & \\ & O_{(b-R) \times (b-R)} \end{pmatrix} U_B^\top M. \quad (96)$$

This means that for all t , the SVD decomposition of X_t is the same. Then with one-step HRP, calculated $X_t = U \Sigma V^\top$ is the SVD decomposition of

$$\hat{X}_\infty := \lim_{t \rightarrow \infty} \hat{X}_t = U_B \begin{pmatrix} I_r & \\ & O_{(b-r) \times (b-r)} \end{pmatrix} U_B^\top M. \quad (97)$$

. With assuming M to be low-rank, \hat{X}_∞ has rank

$$\text{rank}(\hat{X}_\infty) \leq \text{rank}(M) \leq r. \quad (98)$$

which means according to Theorem 3.5 we have

$$\hat{X}_\infty^* := U \begin{pmatrix} I_r & \\ & O_{(b-r) \times (b-r)} \end{pmatrix} U^\top \hat{X}_\infty = \hat{X}_\infty. \quad (99)$$

Then, we calculate the Frobenius norm of the converged result after HRP. In fact, we have

$$\left\| \lim_{t \rightarrow \infty} X_t \right\|_F^2 = \left\| U \begin{pmatrix} I_r & \\ & O_{(b-r) \times (b-r)} \end{pmatrix} U^\top M \right\|_F^2 \quad (100)$$

$$= \left\| \hat{X}_\infty^* \right\|_F^2 + \left\| U \begin{pmatrix} I_r & \\ & O_{(b-r) \times (b-r)} \end{pmatrix} U^\top (M - \hat{X}_\infty) \right\|_F^2 \quad (101)$$

$$+ 2 \text{Trace} \left(\hat{X}_\infty^{*\top} U \begin{pmatrix} I_r & \\ & O_{(b-r) \times (b-r)} \end{pmatrix} U^\top (M - \hat{X}_\infty) \right) \quad (102)$$

$$= \left\| \hat{X}_\infty^* \right\|_F^2 + \left\| U \begin{pmatrix} I_r & \\ & O_{(b-r) \times (b-r)} \end{pmatrix} U^\top (M - \hat{X}_\infty) \right\|_F^2 + 2 \text{Trace} \left(\hat{X}_\infty^{*\top} (M - \hat{X}_\infty) \right) \quad (103)$$

$$\geq \left\| \hat{X}_\infty \right\|_F^2 + 2 \text{Trace} \left(\hat{X}_\infty^\top (M - \hat{X}_\infty) \right) \quad (104)$$

$$= \left\| \hat{X}_\infty \right\|_F^2 + 2 \text{Trace} \left(M^\top U_B \begin{pmatrix} I_r & \\ & O_{(b-r) \times (b-r)} \end{pmatrix} U_B^\top \left(M - U_B \begin{pmatrix} I_r & \\ & O_{(b-r) \times (b-r)} \end{pmatrix} U_B^\top M \right) \right) \quad (105)$$

$$= \left\| \hat{X}_\infty \right\|_F^2 + 2 \text{Trace} \left(M^\top U_B \begin{pmatrix} I_r & \\ & O_{(b-r) \times (b-r)} \end{pmatrix} U_B^\top U_B \begin{pmatrix} O_{r \times r} & \\ & I_{b-r} \end{pmatrix} U_B^\top M \right) \quad (106)$$

$$= \left\| \hat{X}_\infty \right\|_F^2. \quad (107)$$

According to Theorem A.2, we have

$$\mathcal{L}(\lim_{t \rightarrow \infty} X_t) = \mathcal{L}(\hat{X}_\infty). \quad (108)$$

According to Theorem 3.1, we have in expectation:

$$\mathbb{E}_{LSI} \mathcal{L}(\lim_{t \rightarrow \infty} X_t) = \frac{b-R}{2b} \|M\|_F^2. \quad (109)$$

For RSI in matrix sensing, it is equivalent to LSI with X^\top approximating M^\top , thus for RSI we have

$$\mathbb{E}_{RSI} \mathcal{L}(\lim_{t \rightarrow \infty} X_t) = \frac{a-R}{2a} \|M\|_F^2. \quad (110)$$

□

B. Experiment Details

B.1. Detail for NLU tasks

For the GLUE benchmark using T5-base model, we run experiments on a single NVIDIA L40 GPU and report the detailed hyperparameters in Table B.1.

Table 3. Hyperparameter settings for fine-tuning T5-base on GLUE.

	CoLA	MRPC	QNLI	RTE	SST-2	STS-B
Optimizer			AdamW			
Batch size			8			
Learning rate			4×10^{-4}			
Epochs	5	2	2	2	2	2
Dropout			0.05			
LR Scheduler			linear			

B.2. Detail for NLG tasks

For the math reasoning tasks using large language model, we run experiments on four NVIDIA H100 GPU and report the detailed hyperparameters in Table B.2. For prompt in the fine-tuning stage and the inference stage, we use the given prompt template provided by the model.

Table 4. Hyperparameter settings for fine-tuning math reasoning tasks.

	Llama2	Qwen2	Falcon3
Optimizer		AdamW	
Batch size		32	
Learning rate		5×10^{-5}	
Epochs		1	
Dropout		0.05	
LR Scheduler		cosine	
Training data type	float32	bfloat16	bfloat16
Inference data type		bfloat16	
Inference temperature		0.8	
Inference top p		0.95	
Inference max new tokens		512	

C. More Experiment Results

For fine-tuning models on NLG tasks, we present the loss curve for Llama2 in 2, Falcon3 in 3, and Qwen2 in 4.

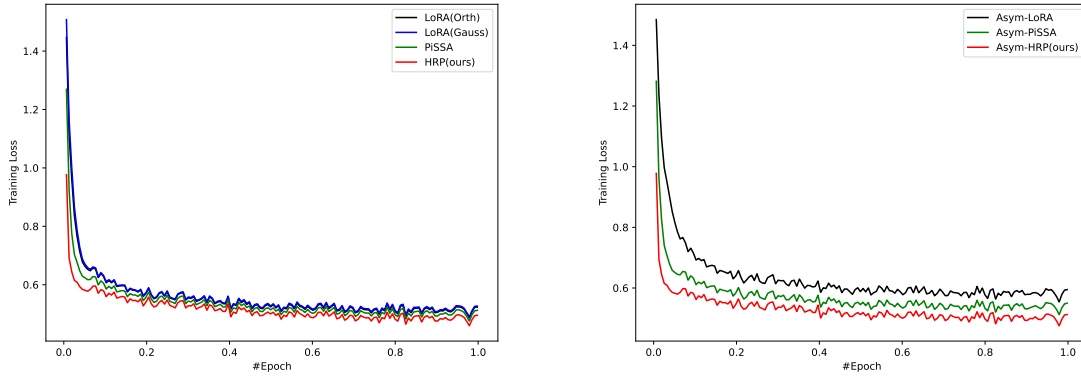


Figure 2. Loss curves for fine-tuning meta-llama/Llama-2-7b-chat-hf on the MetaMathQA. Left: classic LoRA in different initialization strategies. Right: Asymmetric LoRA in different initialization strategies.

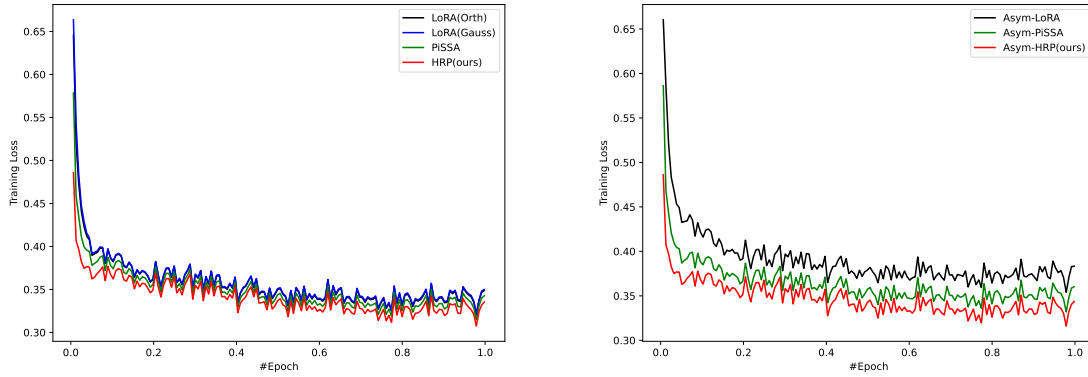


Figure 3. Loss curves for fine-tuning tiuae/falcon-7b-instruct on the MetaMathQA. Left: classic LoRA in different initialization strategies. Right: Asymmetric LoRA in different initialization strategies.

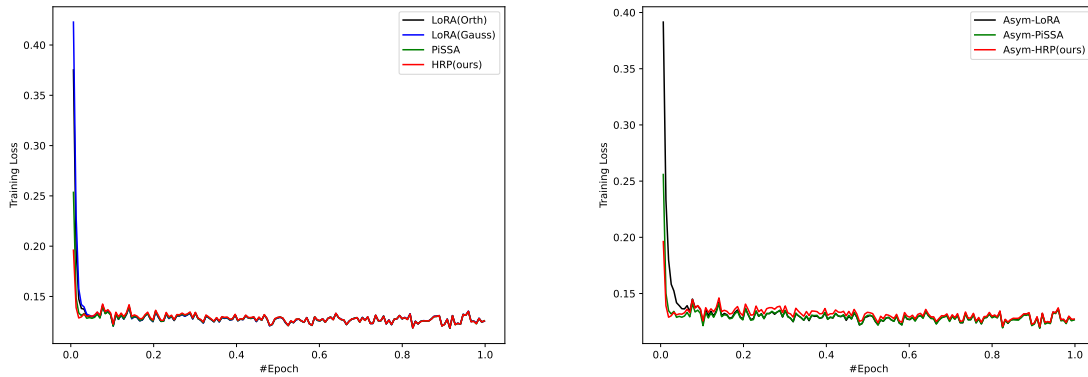


Figure 4. Loss curves for fine-tuning Qwen/Qwen2-7B-Instruct on the MetaMathQA. Left: classic LoRA in different initialization strategies. Right: Asymmetric LoRA in different initialization strategies.